Time-of-flight optical ranging system based on time-correlated single-photon counting

John S. Massa, Gerald S. Buller, Andrew C. Walker, Sergio Cova, Manikam Umasuthan, and Andrew M. Wallace

The design and implementation of a prototype time-of-flight optical ranging system based on the time-correlated single-photon-counting technique are described. The sensor is characterized in terms of its longitudinal and transverse spatial resolution, single-point measurement time, and long-term stability. The system has been operated at stand-off distances of 0.5–5 m, has a depth repeatability of <30 μm, and has a lateral spatial resolution of <500 μm. © 1998 Optical Society of America

OCIS codes: 120.3930, 150.5670, 150.6910, 280.3400.

1. Introduction

The purpose of an optical ranging sensor is to collect three-dimensional coordinate data from object surfaces to provide quantitative information about a target, scene, or environment. Such systems have applications in areas as diverse as precision component inspection, automated assembly, process control, robot navigation, cartography, and satellite ranging. The different types of active optical ranging sensor, and their principles of operation, have been described in detail by Besl.[1] Each of these techniques has its own particular merits, which determine its suitability for use in a specific application. These may include a combination of factors such as measurement precision, single-point acquisition time, stand-off distance, depth of field, safety, and cost.

The time-of-flight method utilizes light pulses emitted from a source, commonly a laser, which travel toward a target and from which a fraction of the signal is scattered back to the sensor, usually along the same optical path. Measurement of the time interval between emission and detection of the pulses gives a direct measurement of the round-trip distance to the target. Because this method permits coaxial alignment of the incident and the return optical paths, examination of complex surfaces with high aspect-ratio (depth/width) features can be achieved without the occlusion problems associated with stereoscopic and triangulation systems. The main disadvantage of current laser-based techniques is the requirement for a sufficiently large return signal from the target to permit an accurate distance measurement. This problem is of particular relevance when one is observing distant or uncooperative targets, and overcoming it often requires the use of expensive and cumbersome high-power laser systems or the placement of retroreflecting spheres on the target.

To overcome this problem we use a sensitive photon-counting technique to monitor the return signal. Time-correlated single-photon counting[2] (TCSPC) is a statistical averaging technique that has single-photon detection sensitivity and picosecond timing accuracy. This technique has been used for a number of years for luminescence decay measurements[3,4] and optical time-domain reflectometry in optical fibers.[5] In a recent publication[6] we demonstrated the application of TCSPC to optical ranging, with the resultant measurements having a repeatability of ± 30 μm at a stand-off distance of ~1 m. Here we describe the design and performance of a stand-alone prototype TCSPC ranging system designed to be used at large (0.5–25-m) distances while remaining eye safe. Specifically, such a system could be used to validate large aircraft structures during manufacture. The system has been characterized in terms of its spatial

J. S. Massa, G. S. Buller, and A. C. Walker are with the Department of Physics, Heriot-Watt University, Riccarton, Edinburgh EH14 4AS, UK. (e-mail for J. S. Massa, j.s.massa@hw.ac.uk). S. Cova is with the Dipartmento di Elettronica e Informazione, Politecnico di Milano, Piazza Leonardo Da Vinci 32, 20133 Milan, Italy. M. Umasuthan and A. M. Wallace are with the Department of Computing and Electrical Engineering, Heriot-Watt University, Riccarton, Edinburgh EH14 4AS, UK.

Received 13 May 1998; revised manuscript received 14 July 1998.

0003-6935/98/317298-07$15.00/0

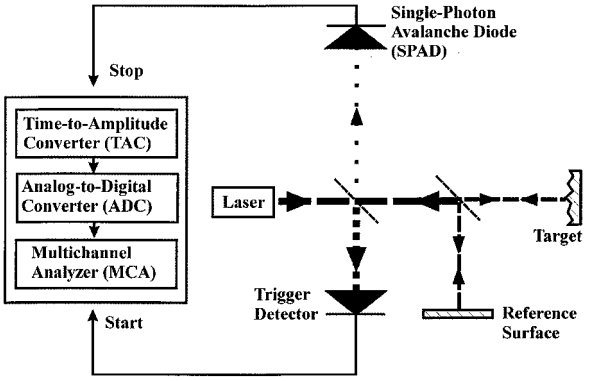

Fig. 1. Schematic of a TCSPC ranging system, indicating the main components.

resolution (both longitudinal and transverse), the speed of data acquisition when one is studying a variety of materials and surface textures, and its long-term stability. The flexible design of the system has permitted us to assess several different optical and electronic configurations to determine the suitability of TCSPC for this application.

2. System Design

Our time-of-flight ranging system uses standard TCSPC techniques and is shown in simplified schematic form in Fig. 1. A fraction ($\sim$2%) of the laser output is split off and provides a timing signal that starts a time-to-amplitude converter (TAC). The remaining laser signal is directed toward the target, and the scattered return signal is routed to a photon-counting detector, which stops the TAC on arrival of the first photon. The TAC produces an analog output signal with an amplitude proportional to the time difference between the start and stop inputs. This signal is then digitized by an analog-to-digital converter and is used to increment the contents of a memory address in the multichannel analyzer, corresponding to the small time interval in which the photon was detected. Because the photon-counting system will utilize only the first photon that arrives at the detector for a given laser pulse, the detection probability must be sufficiently low (in practice, $<$5%) to minimize any multiple-photon events that will distort the statistical distribution of recorded photon arrival times. After many photon-timing events, the multichannel analyzer contains a histogram that accurately represents the probability distribution of arrival times of returning photons. When a high-repetition-rate ($>$100-kHz) source is used, the TAC is normally operated in reverse mode,[7] with the photon-counting detector providing the start signal and the time-delayed trigger providing the stop. This technique affords a much more efficient counting system by starting the TAC only when a photon is detected, and the temporally reversed histogram can be corrected by software. In practice, to minimize drift in the timing system it is necessary to have a reference surface located in the optical head and to make measurements of the distance, Δz, relative to this surface.

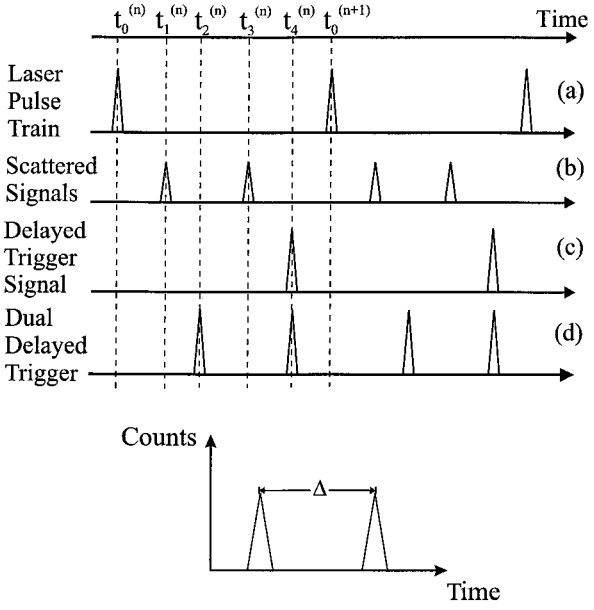

Fig. 2. Timing diagram for the TCSPC ranging system, indicating the temporal positions of the scattered signals from the target and the reference (b) relative to the laser pulse (a). Also shown are the relative positions of the delayed trigger (c) for operation of the TAC in reverse mode and a second trigger signal (d) for use in the dual-trigger scheme. The diagram at the bottom represents the TCSPC histogram that defines the separation of the histogram peaks.

A timing diagram for the photon-counting system, indicating the nth and the n + 1st periods of the laser, is shown in Fig. 2: The optical pulses (a) have a repetition period of $t_0^{(n+1)} - t_0^{(n)}$, whereas the scattered signals from the target and the reference (b) occur at times $t_3^{(n)} - t_0^{(n)}$ and $t_1^{(n)} - t_0^{(n)}$ after the nth laser pulse. The delayed trigger signal for operation of the TAC in reverse mode (c) occurs at time $t_4^{(n)}$ with respect to the laser pulse, and the peak separation on the histogram, Δ, is equal to the true separation of the target and reference signals, $t_3^{(n)} - t_1^{(n)}$. It is worth noting that, because the target and the reference signals in the distribution are well separated, the finite probability of detecting a photon in the first signal will only reduce the area of the second measured signal, without causing distortions in its shape. Thus each of the target and reference signals can count at the maximum statistical rate ($\sim$5% of the laser repetition rate) without being affected by pulse pileup and thus effectively doubling the detection rate.

An alternative configuration for the photon-counting system requires the use of two trigger signals (d) separated in time by $t_4^{(n)} - t_2^{(n)}$ and derived either optically or electrically from the same single trigger signal. In this case the peak separation on the histogram is related to the true separation by

$$\Delta = [t_4^{(n)} - t_2^{(n)}] - [t_3^{(n)} - t_1^{(n)}].$$

The advantage of this second configuration is that the delays of the two trigger signals can be separately

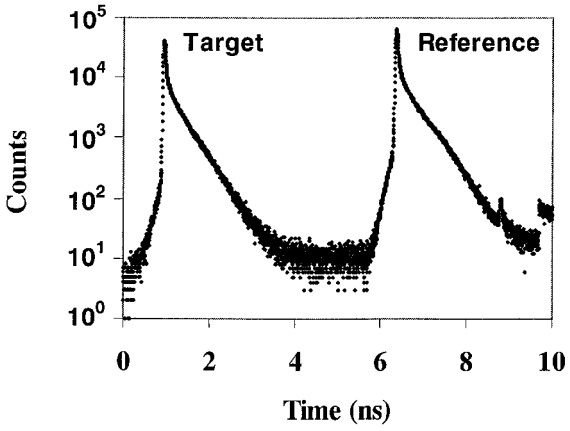

Fig. 3. Log-linear plot of a typical TCSPC histogram obtained from the system and indicating the scattered signals from the target and reference surfaces. The plot contains 4096 time bins, each with a width of 2.44 Ps. The temporal width of each peak is ~60 Ps (FWHM).

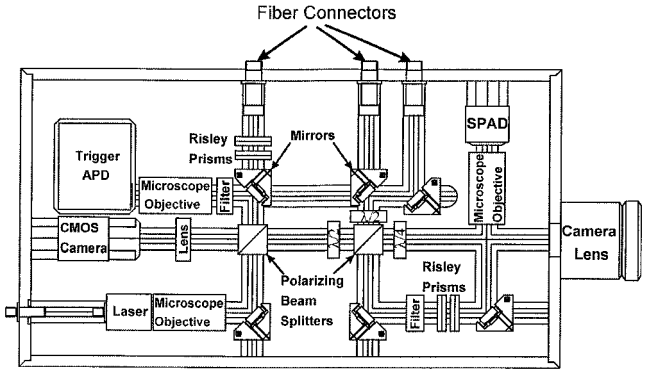

Fig. 4. Plan view of the TCSPC ranging system, indicating the main components. CMOS, complementary metal–oxide semiconductor.

adjusted and, therefore, the position of each peak can be independently and conveniently adjusted within the short time range analyzed by the digital time sorter.

The pulsed optical source used for the time-of-flight system is a passively Q-switched AlGaAs laser diode[8] emitting ~10-ps pulses of ~10-pJ energy at a wavelength of ~850 nm and a repetition rate of 25 MHz. The photon-counting detector is a silicon single-photon avalanche diode[9] (SPAD), which gives a single-photon timing accuracy of ~20 ps and can operate at count rates of as much as ~2 MHz by use of an active quenching circuit. Compared with photomultipliers, these detectors exhibit superior photon-detection efficiency and a faster, cleaner time response.[10,11] The TAC, the analog-to-digital converter, and the multichannel analyzer are integrated onto a single plug-in card (Becker & Hickle SPC-300) for an IBM-compatible personal computer, and this system has a maximum data acquisition rate of >2 MHz. A typical plot of a histogram for this system, shown in Fig. 3, has 4096 time bins, each corresponding to a 2.44-ps time interval, and contains two peaks that represent scatter from the target and reference surfaces. The temporal width of the peaks is ~60 ps full width at half-maximum.

For maximum timing accuracy it is necessary to operate the TAC on the smallest time range and at a high-gain setting. This procedure leads to a rather restricted time window of typically ~10 ns within which the reference and target peaks must be fitted, and consequently the reference surface must be within ±1.5 m of the target to permit a measurement to be made. For distances greater than this, different lengths of single-mode polarization-maintaining optical fiber are used to ensure that the reference signal remains in the same time window as the target signal. If a dual-trigger scheme is employed as described above, and the second trigger signal is derived electronically by use of a switchable delay box, then only one length of optical fiber needs to be used, and the process becomes much simpler.

We achieve the mechanical stability required for the optical system by mounting the components upon a 30-mm-thick, glass-filled nylon base plate with lateral dimensions of 360 mm × 200 mm. The rigidity is further increased by four interlocking aluminum side plates and a lid to provide a box construction. This arrangement affords the components some degree of protection from the external environment and also provides a light-tight enclosure for the detection system. The base plate has V grooves machined into the surface to take optical components (lenses, prisms, etc.) mounted in steel rings (or cylinders) of 25-mm diameter. The layout of the base plate, shown in Fig. 4, defines the optical paths within the system and was designed to permit maximum flexibility in the investigation of several different optical configurations. The optical axis defined by the V grooves lies 10 mm above the surface of the base plate and permits movement of the optical components only by rotation about or translation along the axis. Iron rods glued into the bottoms of the grooves allow the components to be held magnetically in position. The physical size of the camera and the x–y adjustments necessary to center the SPAD on the optical axis mean that these components have to be mounted in 30-mm-diameter cylinders. We accommodate this constraint by machining out the base plate and inserting cylindrical steel rods to allow the components to slide along a short length of modified track while they are centered on the same optical axis as the V grooves. The base plate also accommodates the trigger avalanche photodiode (APD), aligned to allow the active area of the device to be centered on the optical axis of the appropriate V groove. Mounted in the rear panel are various connectors for the laser drive current, photon-counting signals, and dc bias supplies for the different components. Radial variable-frequency oscillator single-mode fiber connectors that contain integral coupling lenses are mounted into one of the side panels, at positions centered on the optical axis, to permit the simple interchange of different lengths of fiber optical delay. An

aperture located in the front panel, centered on the optical axis, permits output from laser pulses and the collection of scattered light from the target. A steel flange bolted around the aperture is included for the attachment of an external lens with a Pentax K mount fitting.

The base-plate optical system is an infinite conjugate arrangement with the laser, the SPAD, the trigger APD, the camera, and the optical fiber ends positioned in the respective focal planes of various lenses. Collimation of the laser is achieved with a 20× microscope objective (N.A., 0.54), which defines an on-axis beam diameter of ≤8 mm within the system. Rotation of the laser mount about the optical axis can be used to rotate the polarization state of the light incident upon the first beam splitter and thus to control the signal transmission/reflection ratio. A half-wave plate is used to control the amount of light from the reference fiber that reaches the SPAD, and a quarter-wave plate converts the polarization of the laser pulse, leaving the optical head circular so the collected scattered signal from target can be efficiently polarization routed onto the SPAD.

For initial characterization of the system, a plano–convex singlet of 1-m focal length and 8-mm diameter was used to focus the laser spot onto the target (at a fixed distance of 1 m) and to collect the scattered signal. This fixed-focus, low-N.A. system, operating at $f/125$, was used to explore the feasibility, in terms of signal return and laser spot size, of operating the system at longer stand-off distances, e.g., ~25 m. For such longer-range targets the optical system will use an output–input lens of ~100-mm diameter and therefore will be operating at a similar ~$f/250$ aperture.

On the basis of geometric magnification, the 1-m lens should give a spot of diameter ~250 μm on a 1-m distant target. The size of this spot is approaching the diffraction limit. In the plane of the SPAD the image of the backscattered light is formed with a 10× microscope objective (N.A., 0.25) and will be <4 μm in diameter, which can be compared with the active diameter of the smallest SPAD device (~7 μm). We achieved precise alignment by rotating pairs of glass prisms (wedge angle, ~7 min) about the optical axis in regions where the beam is collimated. For the 10× microscope objective lens working at an infinite conjugate ratio, rotating the prisms deflects the image in the focal plane by ~50 μm. The small active diameter of the SPAD permits spatial filtering of the detected signal to minimize spurious reflections that originate from the internal optical components.

Two multiple-cavity interference filters are used to prevent background light from reaching the SPAD or the trigger APD, which could cause degradation of measurements made of illuminated targets. Each of these filters is centered at 855 nm, with a passband of ~40 nm and a peak transmission of ~80%. All optical transmission components such as lenses, beam splitters, prisms, wave plates, and filters are antireflection coated (reflection, <0.5% per surface) for the laser wavelength. The dielectric mirrors used to fold the optical path have a reflectivity of >99% at the laser wavelength.

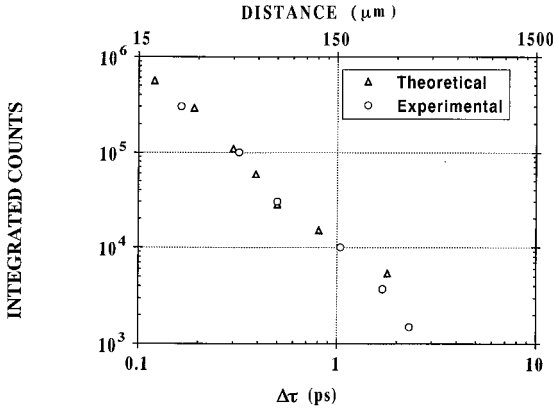

Fig. 5. Distance repeatability and temporal repeatability, Δτ, versus the integrated number of counts in the TCSPC histogram. Circles, standard deviation for repeated experimental measurements on a 1-m distant target; triangles, results of a Monte Carlo simulation.

3. System Performance

The performance of the system can be divided into four categories: longitudinal spatial resolution, transverse spatial resolution, single-point measurement time, and long-term stability.

The longitudinal spatial resolution is determined by the accuracy with which laser pulses can be timed to travel from the optical head to the target and back again. This accuracy depends on two factors: the single-photon timing accuracy σ and the number of single-photon measurements N made for each point on the target. The former is determined by a combination of the laser pulse width and the response width of the detection system. The latter simply leads to an improvement in the single-photon timing accuracy by statistically averaging over many measurements. For the measurements made in the previous study[6] and shown in Fig. 5, the statistically improved accuracy $\bar{\sigma}$ was found to follow the usual equation for the error on the mean of a large number of measurements in the presence of uncorrelated noise, given by

$$\bar{\sigma} = \sigma/\sqrt{N}. \tag{1}$$

Thus for a single-photon timing accuracy σ ~ 50 ps (which is typical of our system), and for the number of photon events $N \sim 10^6$ in each of the target and reference peaks $\bar{\sigma} \sim 70$ fs, which corresponds to a distance measurement accuracy of ~10 μm. A typical satelite laser ranging system based on photon counting uses a similar response detector with $N <$ 10, which corresponds to a distance accuracy of a few millimeters.

The transverse spatial resolution is determined, with this optical configuration, by the size of the laser spot on the target; it is ~250 μm for the fixed-focus $f/125$ output lens with the target at a distance of

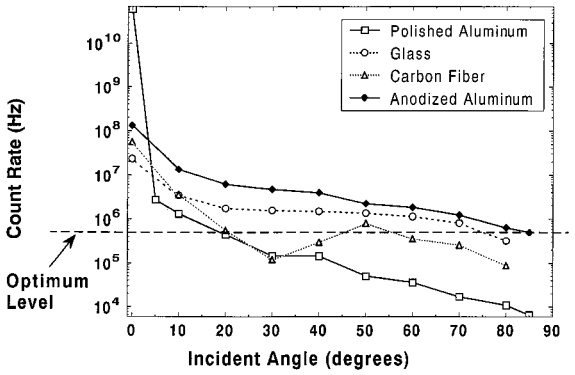

Fig. 6. Measured detection rate of backscattered photons as a function of incident angle for various materials. The collection system was operating at $f/125$, and the laser repetition rate was 10 MHz. The dashed line marks the maximum signal level acceptable for correct operation of the system, at which the maximum signal-to-background ratio is attained.

$\sim$1 m. Alternatively, with a 200-mm $f/4$ camera lens at the output a spot size of $\sim$500 μm was demonstrated at a distance of $\sim$5 m. This resolution is expected to improve with modification of the camera-lens mounting scheme and better coupling optics. For a diffraction-limited system, a transverse resolution of $\sim$1 mm can be expected for targets at 25-m distance.

The time taken to make a distance measurement at a single point is determined by both the backscattered signal intensity and the precision required. As shown in Fig. 5, the repeatability is determined by the number of photon events recorded in the histogram. The backscattered signal detection rate S depends on two adjustable parameters: the laser repetition rate R and the number (optical energy) of photons per pulse N_v. The detection rate also depends on fixed parameters that result from the system design, which control the probability P_d that an emitted photon be detected and, therefore, control the mean number of detected photons per pulse N_d:

$$N_d = N_v P_d. \tag{2}$$

The output routing efficiency of the laser signal, η_{Out}, is the fraction of the emitted laser signal transmitted through the optical head. It is determined by the laser collimation optics, losses owing to surface reflections at components, transmission of filters, leakage through beam splitters, and the amount of light split off for the trigger APD and the optical reference. Similarly, the receiving routing efficiency, η_{Rec}, is the fraction of the signal scattered from the target and entering the collection lens that reaches the detector and is determined by factors similar to those for η_{Out}. Other factors that affect the detection rate are the surface nature of the target material and the geometry of the measurement. $\eta_{\mathrm{Scat}}(\theta)$ is the fraction of the signal backscattered for an incident angle θ and is determined by the surface properties of the material. If, as a first approximation, Lambertian scattering from the target is assumed, then $\eta_{\mathrm{Scat}}(\theta)$ is proportional to $\cos^2\theta$. The fractional solid angle subtended by the collection lens at the target is $1/[8(f_{\mathrm{Col}}/\#)^2]$, where $f_{\mathrm{Col}}/\#$ is the collection f-number of the system. The quantum efficiency of the detector is η_{Det}, and thus the probability P_d is

$$P_d = \frac{\eta_{\mathrm{Out}}\eta_{\mathrm{Rec}}\eta_{\mathrm{Det}}\eta_{\mathrm{Scat}}}{8(\mathrm{f}_{\mathrm{Col}}/\#)^2}. \tag{3}$$

The backscattered signal-detection rate S is given by the product of the laser repetition rate and the probability of detecting one or more photons per pulse, that is, unity minus the probability of zero detected photons $\exp(-N_d)$:

$$S = R[1 - \exp(-N_d)]. \tag{4}$$

For $N_d \ll 1$ the backscattered signal-detection rate S equals the backscattered photon-detection rate R_p:

$$S = RN_d = R_p. \tag{5}$$

One can evaluate the available backscattered signal intensity for typical materials used in aircraft manufacture by measuring the backscattered signal-detection rate S as a function of incident angle. Whenever necessary, calibrated neutral-density filters can be used for reducing the detected intensity and correctly employing Eq. (5) in all cases.

Figure 6 shows the backscattered photon-detection rate thus evaluated in angular scatter measurements made with this system on a range of sample target materials, normalized to take into account the attenuation of neutral-density filters. The system parameters for these measurements were $R = 10$ MHz, $N_v \sim 5 \times 10^7$, $f_{\mathrm{Col}}/\# = 125$, $\eta_{\mathrm{Out}} \approx \eta_{\mathrm{Rec}} \sim 0.7$, and $\eta_{\mathrm{Det}} \sim 0.05$. The Lambertian scattering formula gives the detection rate as $\sim 5 \times 10^7$, assuming these conditions and that $\theta = 45°$. This formula clearly does not apply to polished metals because $\eta_{\mathrm{Scat}}(\theta)$ is a strong function of θ, and most of the incident laser signal will be reflected specularly with only a small fraction scattered. For the less smooth materials the specular component is much less pronounced, and for incident angles of $>10°$ there is a much smaller variation of the detection rate with angle, indicating that the Lambertian scattering approximation is much closer for these materials.

In the TCSPC ranging system the backscattering signal is superposed upon a constant background because of the uncorrelated dark-count pulses generated in the SPAD detector with counting rate D. The signal-to-background ratio (SBR) is the ratio of the mean number N_d of detected photons per pulse to the mean number N_B of dark counts that occur in a time interval equal to the measured temporal response width of the source, τ_{peak}. Taking into account Eq. (5), one has

$$\mathrm{SBR} = \frac{N_d}{N_B} = \frac{S}{RD\tau_{\mathrm{peak}}}. \tag{6}$$

As the signal intensity N_d should not exceed $N_{d\mathrm{MAX}} \sim 0.05$ (to avoid distortion of the measured statistical distribution of photon arrival times), the maximum value of the SBR is, independently of the source repetition rate,

$$\mathrm{SBR}_{\mathrm{MAX}} = \frac{0.05}{D\tau_{\mathrm{peak}}}. \tag{7}$$

For this system, typical values are $D \sim 200$ Hz (for room-temperature operation of a silicon SPAD) and $\tau_{\mathrm{peak}} \sim 60$ ps, so it is $N_B \sim 1.2 \times 10^{-8}$ and the maximum value is $\mathrm{SBR}_{\mathrm{MAX}} \sim 4 \times 10^6$. One can appreciate the wide dynamic range of the system by evaluating the minimum measurable signal, that is, the signal intensity that corresponds to unit value of the signal-to-noise ratio (SNR). The SNR is the ratio of the recorded photon counts to the root-mean-square fluctuation of the recorded total (photon plus dark) counts and depends on the total number of laser pulses $N_L = RT_m$ in the TCSPC averaging run over the total measurement time T_m:

$$\mathrm{SNR} = \frac{N_L N_d}{(N_L N_d + N_L N_B)^{1/2}} = \sqrt{N_L}\,\frac{N_d}{\sqrt{N_d + N_B}}. \tag{8}$$

In the averaged measurement, as long as $N_L N_B \ll N_L N_d$, the background contribution to the fluctuation is negligible and the SNR is dominated by the photon statistics. Therefore the minimum measurable signal $N_{d\mathrm{min}}$ is given by

$$N_{d\mathrm{min}} \cong \frac{1}{N_L} \tag{9}$$

as long as

$$N_L N_B \ll 1. \tag{10}$$

In this system, this limitation corresponds to $N_L \ll 8 \times 10^7$. Thus with $N_L \sim 10^7$ one has $N_{d\mathrm{min}} \sim 10^{-7}$, which with $N_{d\mathrm{MAX}} = 0.05$ gives a dynamic range of the measurement $N_{d\mathrm{MAX}}/N_{d\mathrm{min}} = 5 \times 10^5$ and corresponds to a minimum rate of detected photons $R_{p\mathrm{min}} = 1$ Hz for a laser pulse repetition rate $R = 10$ MHz. However, to attain high precision in the distance measurement may require an integrated number of photon counts $N_L N_d \sim 10^6$, as illustrated in Fig. 5. The corresponding number of laser pulses N_L may largely exceed the limit of Eq. (10); that is, it may be

$$N_L \gg \frac{1}{N_B}. \tag{11}$$

In such cases the photon contribution to the fluctuation is negligible and the SNR is dominated by the background statistics:

$$\mathrm{SNR} \cong \frac{N_L N_d}{\sqrt{N_L N_B}} = \sqrt{N_L}\,\frac{N_d}{\sqrt{N_B}}, \tag{12}$$

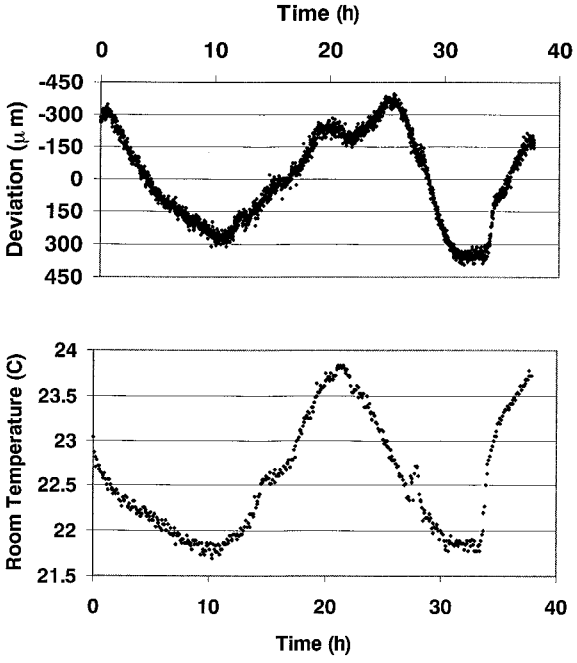

Fig. 7. Stability plot, showing the deviation of a fixed distance measurement as a function of time. Also shown is the room-temperature variation.

and in this instance the minimum measurable signal $N_{d\mathrm{min}}$ is given by

$$N_{d\mathrm{min}} \cong \frac{\sqrt{N_B}}{\sqrt{N_L}}. \tag{13}$$

In this system, with a counting run lasting $T_m = 10$s at a laser pulse repetition rate $R = 10$ MHz, one has $N_L \sim 10^8$, and the minimum signal is $N_{d\mathrm{min}} \sim 10^{-8}$; this corresponds to a minimum rate of detected photons $R_{p\mathrm{min}} = 0.1$ Hz and, with $N_{d\mathrm{MAX}} = 0.05$, to a dynamic range of the measurement $N_{d\mathrm{MAX}}/N_{d\mathrm{min}} = 5 \times 10^6$.

For the angular scatter results shown in Fig. 6 the source repetition frequency was 10 MHz; thus the maximum allowable detected signal intensity corresponded to a detection rate of ~500 kHz. It can be seen that this signal level was achieved for all the materials tested, even at large incident angles, with the exception of the polished aluminum. In the lat-

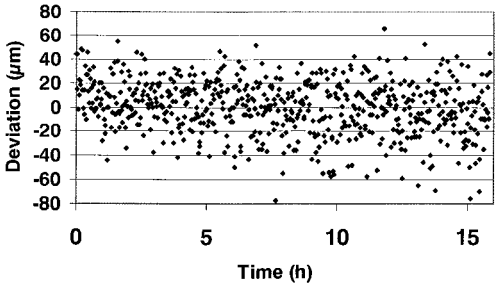

Fig. 8. Stability plot, showing the deviation of a fixed distance measurement as a function of time for a temperature-stabilized system.

ter case at angles of >25° the signal, although it is smaller than the maximum allowable level, is still much greater than the minimum detectable level; thus measurements can still be made by use of a longer acquisition time. With the source repetition frequency increased to 25 MHz the optimum data acquisition rate and the backscattered signal from the target will be increased accordingly. With reference to Fig. 5, this increase will permit 1 single-point measurement with a precision of ~10 μm or 100 single-point measurements with a precision of ~150 μm every second.

High system stability is needed if multipoint scans are to be made of complex surfaces over long periods of time without degradation of relative precision. Our measurements have shown that the system may drift by several picoseconds over a period of several hours, and this appears to correlate with changes in the ambient temperature. The drift effect can be clearly seen in Fig. 7, which shows a series of measurements of the same distance (approximately 1 m) over a period of several hours and a maximum (peak-to-peak) drift of ~600 μm. We achieved this level of stability by calculating the separation between the target and reference return pulses from the separation of the centroids of the outer peaks of the autocorrelation function. If the reference signal is not used and the position is estimated only from the time of the target return relative to the electronic timing trigger, then the maximum peak-to-peak drift is ~5 mm. Also shown in Fig. 7 is the ambient temperature measured over the same period. The observed drift has a remarkable correlation with the ambient-temperature variation. Figure 8 shows a similar stability plot that we obtained by controlling the ambient temperature; in this case the drift has been eliminated, giving a standard deviation of only ±30 μm about the mean distance. We carried out detailed tests to ascertain the sensitivity to temperature of individual components of the system. The experimental results clearly showed that drift is correlated mainly to variations of the laser driver temperature. Therefore the engineered version of the system is designed to include control and stabilization of the laser driver temperature to eliminate drift in the measurements without the need to stabilize the temperature of the whole ambient.

4. Conclusions

The implementation of a time-of-flight optical ranging system by the time-correlated single-photon-counting (TCSPC) technique has been described. The system uses a *Q*-switched laser diode source and a silicon single-photon avalanche diode (SPAD) detector. The depth repeatability of the system is ≤30 μm, and the transverse spatial resolution is <500 μm at a distance of 5 m. The high-power laser sources, efficient optical routing, and single-photon-detection sensitivity permit the measurement of arbitrary materials and surfaces by use of minimal collection optics ($f/125$) without the need to employ retroreflectors. This prototype system has provided significant information on the practicality of using this technique, and we are currently building a second, automated system to permit measurements at distances of as much as 25 m in a practical engineering environment.

This study forms part of a collaboration between the Departments of Physics and of Computing and Electrical Engineering of Heriot-Watt University, British Aerospace-Sowerby Research Centre, and Edinburgh Instruments, Ltd., and has been supported financially by the UK Engineering and Physical Sciences Research Council through its Integrated Machine Vision Initiative. The authors acknowledge the financial support of the UK Royal Society Joint Project Fund, NATO Collaborative Research grant 9202218, and INTAS (International Association for the Promotion of Cooperation with Scientists from the Independent States of the former Soviet Union) grant 93-2687. The passively *Q*-switched lasers were provided by E. L. Portnoi and co-workers of the A. F. Ioffe Institute, St. Petersburg, Russia.

References

1. P. J. Besl, "Active optical imaging sensors," Mach. Vision Appl. **1,** 127–152 (1988).
2. D. V. O'Connor and D. Phillips, *Time Correlated Single Photon Counting* (Academic, London, 1984).
3. J. S. Massa, G. S. Buller, A. C. Walker, J. L. Oudar, E. V. K. Rao, B. G. Sfez, and R. Kuselewicz, "Evidence of carrier confinement in nonlinear GaAs/AlGaAs multiple quantum well microresonators fabricated using alloy mixing techniques," Appl. Phys. Lett. **61,** 2205–2207 (1992).
4. J. S. Massa, G. S. Buller, A. C. Walker, J. Simpson, K. A. Prior, and B. C. Cavenett, "Photoluminescence decay measurements of *n*- and *p*-type doped ZnSe grown by molecular beam epitaxy," Appl. Phys. Lett. **64,** 589–591 (1994).
5. G. Ripamonti, F. Zappa, and S. Cova, "Effects of trap levels in single-photon optical time-domain reflectrometry—evaluation and correction," J. Lightwave Technol. **10,** 1398–1402 (1992).
6. J. S. Massa, A. M. Wallace, G. S. Buller, S. J. Fancey, and A. C. Walker, "Laser depth measurement based on time-correlated single-photon counting," Opt. Lett. **22,** 543–545 (1997).
7. B. T. Turko, J. A. Nairn, and K. Sauer, "Single photon timing system for picosecond fluorescence lifetime measurements," Rev. Sci. Instrum. **54,** 118–120 (1983).
8. Z. I. Alferov, A. B. Zuravlev, E. L. Portnoi, and N. M. Stel'makh, "Picosecond pulses from *Q*-switched heterostructure injection lasers," Sov. Tech. Phys. Lett. **12,** 452–453 (1986).
9. S. Cova, M. Ghioni, A. Lacaita, C. Samori, and F. Zappa, "Avalanche photodiodes and quenching-circuits for single-photon detection," Appl. Opt. **35,** 1954–1976 (1996).
10. A. Lacaita, M. Ghioni, and S. Cova, "Double epitaxy improves single-photon avalanche-diode performance," Electron. Lett. **25,** 841–843 (1989).
11. S. Cova, A. Lacaita, M. Ghioni, G. Ripamonti, and T. A. Louis, "20ps timing resolution with single photon avalanche diodes," Rev. Sci. Instrum. **60,** 1104–1110 (1989).